Optical Society of America. Bing Yu and Anbo Wang, "Grating-Assisted Demodulation of Interferometric Optical Sensors," Appl. Opt. 42, 6824-6829 (2003). doi: 10.1364/ao.42.006824

Grating-assisted demodulation of interferometric optical sensors

Bing Yu and Anbo Wang

Accurate and dynamic control of the operating point of an interferometric optical sensor to produce the highest sensitivity is crucial in the demodulation of interferometric optical sensors to compensate for manufacturing errors and environmental perturbations. A grating-assisted operating-point tuning system has been designed that uses a diffraction grating and feedback control, functions as a tunable-bandpass optical filter, and can be used as an effective demodulation subsystem in sensor systems based on optical interferometers that use broadband light sources. This demodulation method has no signal-detection bandwidth limit, a high tuning speed, a large tunable range, increased interference fringe contrast, and the potential for absolute optical-path-difference measurement. The achieved 40-nm tuning range, which is limited by the available source spectrum width, 400-nm/s tuning speed, and a step resolution of 0.4 nm, is sufficient for most practical measurements. A significant improvement in signal-to-noise ratio in a fiber Fabry–Perot acoustic-wave sensor system proved that the expected fringe contrast and sensitivity increase.

OCIS codes: 060.2370, 050.1950, 070.6020.

1. Introduction

Fiber-optic interferometers, especially fiber Fabry–Perot interferometers (FFPI), have found increased applications in the past decade for the detection and measurement of a large variety of physical parameters, such as temperature,[1–4] vibration,[1,5] pressure,[3,4,6,7] acoustic waves,[1,5,8–11] and strain.[12,13] Many interferometric sensors operate over the linear region of an interference fringe.[1,3,4,8,9,11] Compared with sensors that use fringe counting,[5,9,11] sensors that operate in the linear region have the advantages of a linear transfer function, no ambiguity in fringe direction, simple signal processing, and highest sensitivity at the quadrature point (Q point). They are, therefore, suitable for detection of small optical path differences (OPDs) and wideband applications. However, confining the operation to the linear region places difficult manufacturing constraints on the sensor head by requiring that the initial cavity length be positioned at the Q point or sometimes at one end of a linear region of the transfer function.[6] The sensors also suffer from signal fading caused by environmental perturbations, such as temperature changes, which may drive the sensors out of the linear region. The drifts are even more critical for Fabry–Perot (F-P) sensors; medium- or high-finesse F-P cavities are often necessary for higher measurement sensitivity[1,11] because of their steeper fringe slopes. Therefore, poor control of the operation point has been a major factor that limits the practical application of interferometric optical sensors in the sensor industry.

Several techniques have been developed by various researchers to stabilize the Q point, for example, intentionally applying an acoustic bias,[1] tuning the static OPD in stages,[14] and using a tunable light source,[8,9] quadrature phase-shifted demodulation or dual-wavelength interrogation,[5,6,12,15] or direct spectrum detection.[6,13,16,17] In the acoustic bias method, the low-frequency component output of a FFPI acoustic-wave sensor was compared with a constant voltage corresponding to the setting operating point, and the difference was used to adjust the acoustic bias through a voice coil. This method does compensate for environmental drifts, but adjusting the operating point with a voice coil limits its use only to acoustic detection, and the coil may cause extra noise. A static OPD is tuned in a Mach–Zehnder interferometer by use of a fiber stretcher. The quadrature point nearest maximum visibility can be locked with

The authors are with the Center for Photonics Technology, Virginia Polytechnic Institute and State University, 460 Turner Street, Blacksburg, Virginia 24061-0287. B. Yu's e-mail address is biyu@vt.edu.

Received 29 May 2003; revised manuscript received 8 August 2003.

0003-6935/03/346824-06$15.00/0

a feedback-control servo system, and a temperature drift from 25 °C to 55 °C has been successfully compensated for. However, tuning the OPD may cause excess power fluctuation in the fiber, and it is not suitable for use with sensors with F-P interferometers. Adjusting the operating point by changing the bias current of a tunable laser diode is another effective approach that has been used by many researchers. The disadvantages of using a tunable laser are its optical power fluctuation, high sensitivity to backreflection, laser mode hopping, and high cost. Quadrature phase-shifted demodulation, or dual-wavelength interrogation, was originally developed by Murphy *et al.*[12] to solve problems of a nonlinear transfer function and directional ambiguity in extrinsic F-P sensors, but it may also be used for the demodulation of sensors operating in the linear regions. However, it is possible that both channels operate away from their optimal Q points at the same time, even if a 90° phase shift can be maintained during the measurement, which is as hard as to control the operating point itself.

Strictly speaking, the spectrum detection method should not be categorized into a kind of operating-point stabilizing method, though linear response can be achieved.[13] Direct spectrum detection uses a diffraction grating or a Fizeau interferometer, and the modulated broadband spectrum is detected by a CCD array and analyzed by a signal-processing unit. This procedure is also called white-light interferometry and actually does not need to control the operating point of an interferometric sensor. It provides an absolute and accurate value of the OPD in a sensing interferometer and is insensitive to power and spectral fluctuations of the light source. Its major disadvantage is that it is not suitable for real-time detection of broadband signals such as acoustic waves and high-frequency pressure because a large amount of time is required for processing the huge amounts of data from a CCD array. Another disadvantage of spectrum detection is its high cost, especially for sensors operating in the near-infrared region, where expensive detector arrays must be used.

In this paper we present an alternative demodulation technique with operation-point tuning by use of a diffraction grating with feedback control, called grating-assisted operating-point tuning (GA-OPT). This demodulation method has no ac bandwidth limit, a high tuning speed, a large tunable range, increased interference fringe contrast, and the potential for absolute optical-path-difference measurement. An experiment in which a fiber F-P acoustic-wave sensor system is used to prove the feasibility of the design is also presented.

2. Wavelength Dependence of Operation Points

Interferometric-intensity-based detection is a widely used demodulation technique in optical interferometric sensors such as fiber F–P interferometers, Mach–Zehnder, and Sagnac sensors. When a monochromatic light of wavelength λ is used to interrogate the sensors, the optical intensity of the two-beam interference between the sensing beam and the reference beam can be expressed as

$$I = I_1 + I_2 + 2\sqrt{I_1 I_2}\cos\phi, \tag{1}$$

where I_1 and I_2 represent the optical intensities of the sensing beam and the reference beam, respectively, and

$$\phi = 2\pi(nl)/\lambda \tag{2}$$

is the phase difference caused by the OPD nl between the two beams, where n is the refractive index of the medium and l is the physical path difference. The optical intensity arriving at the photodetector is a simple cosine function, called interference fringes, of nl, which is a function of perturbations in the measurant and the background. Obviously, sensors have zero sensitivity at the peaks or the valleys of the fringes, and the maximum sensitivity and the most nearly linear response at the Q points, where $\phi = \pi/2 + m\pi$, $m = 0, 1, 2, \ldots$. It is of absolute advantage to design a sensor operating at the Q points for the highest sensitivity and the lowest signal distortion. However, any sensor fabrication tolerance, temperature-induced drift, or other environmental perturbation can easily drive a sensor away from the Q points. Notice that the interference fringes and thereby the Q points are wavelength dependent for all interferometers; one may dynamically control the operation points by tuning the wavelength of the interrogation lights to compensate for the phase drifts, that is,

$$\Delta\phi = \Delta\phi_{(nl)} + \Delta\phi_\lambda = \frac{2\pi}{\lambda}\Delta(nl) - \frac{2\pi(nl)}{\lambda^2}\Delta\lambda = 0, \tag{3}$$

or

$$\Delta\lambda = \frac{\lambda}{(nl)}\Delta(nl), \tag{4}$$

where $\Delta\phi_{(nl)}$ and $\Delta\phi_\lambda$ are the phase changes caused by environmental disturbance $[\Delta(nl)]$ and wavelength tuning $[\Delta\lambda]$. Usually nl is at least 1 order larger than λ, which means that a large drift can be compensated for by a relatively small change in the wavelength. The wavelength tuning can be achieved by use of a tunable laser, though this may cause some problems such as optical power fluctuation and sensitivity to backreflections.

For a broadband light source, the wavelength dependence of the interference fringe is much more complex than for a monochromatic source. The interference fringes are determined not only by the central wavelength but also by the spectrum width of the interrogation lights. The total optical intensity arriving at the photodetector has to be computed by integration over the whole spectrum of the light source. Figure 1 is a theoretical calculation of the wavelength dependence of the interference fringes at

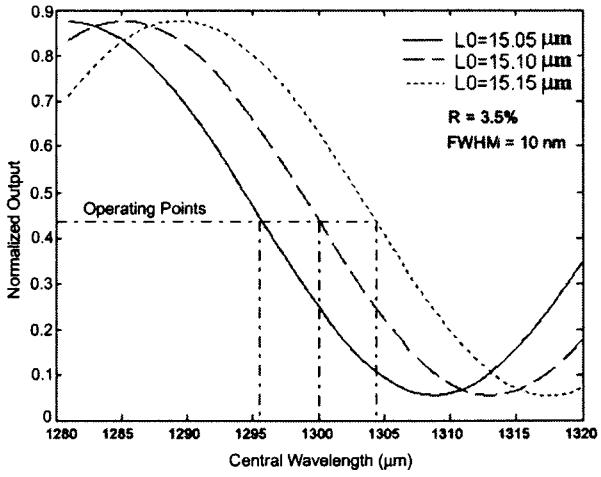

Fig. 1. Theoretical calculation of the wavelength dependence of operation points. R, reflectivity.

three cavity lengths ($L0$) of a low-finesse FFPI sensor,[11] where a 1300-nm light source of a 35-nm (3-dB) spectral width was used, the output was normalized to the source intensity distribution, and the bandwidth of the interrogation lights was limited to $2\Delta\lambda = 10$ nm. For example, if the OPD, for any reason, changes from $L0 = 15.05$ to 15.15 μm, one can track the operation point by tuning the central wavelength from 1.296 to 1.304 μm. The central wavelength of the interrogation light can be tuned by use of GA-OPT, as is discussed in Section 3.

3. Grating-Assisted Operation-Point Tuning

A schematic illustration of a white-light interferometric sensor system based on GA-OPT is shown in Fig. 2. Operation-point tuning is achieved with two collimators, a diffraction grating, a short piece of multimode fiber (MMF), a photodetector, a preamplifier, a computer with a data-acquisition card, and a motorized rotary stage and its driver. The light from a broadband source is launched into a single-mode fiber (SMF), propagates through a 3-dB coupler, and arrives at an interferometric sensor, where it is modulated by the perturbation measurand. The phase-modulated light propagates back through the same 3-dB coupler and reaches the first collimator. The collimated light beam illuminates

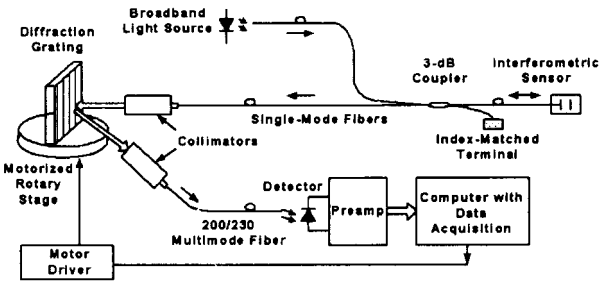

Fig. 2. Schematic diagram of a FFPI sensor system based on GA-OPT.

a diffraction grating, which can be rotated by a motorized rotary stage with high resolution (~0.2 mrad). The −1st diffractions collected by a second collimator are focused into a 200–230-μm MMF, and only part of the total spectrum ($\lambda \pm \Delta\lambda$) can be collected by the MMF.

Instead of a SMF or a detector, a short MMF is used to increase the reception area and to facilitate the spectrum monitoring with an optical spectrum analyzer. The MMF can be removed and the detector can be placed on the focal point of the receiving collimator with a penalty of less flexibility. A transimpedance preamplifier converts the photocurrent into voltage, and a subsequent divider separates the signal into dc and ac components, which are amplified and filtered further. A computer with a data-acquisition card is used to record and to calibrate the dc and ac signals. The calibration reference, a representation of the original optical intensity distribution, is an output-position curve obtained by scanning of the whole wavelength range with a cleaved fiber, instead of a sensor, connected.

The calibrated ac signals directly represent the absolute value of the ac information of the measurand, and the frequency response is limited only by the sensor head and the bandwidth of the electronics. The calibrated dc signals represent the current operation point on the transfer function. Ideally, this dc voltage (V) should to be equal to the setting point (V_0), most likely the Q point. However, any change in manufacturing tolerance and environment may cause an undesired change of the OPD of the sensor and thereby a drift of dc voltage V. The difference ΔV between the dc output and the setting point is the control signal that can be used to adjust the position of the grating, and therefore the central wavelength of the interrogation lights, through a motorized rotary stage. By this feedback control, the optimal operation point can be dynamically maintained, and the dc signal may also be recovered from the position of the grating if environmental effects can be determined. Obviously, the tuning range is limited only by the source spectrum, and the dc accuracy is limited by the resolution and the repeatability of the rotary stage.

According to the grating equation, the relationship between the incident beam and the −1st diffracted beam can be expressed as

$$\sin(A) + \sin(B) = \lambda/d, \tag{5}$$

where A is the incident angle of the light beam from the input collimator to the normal of the grating surface, B is the angle of the −1st diffraction to the normal of the grating surface, λ is the wavelength of light in air, and d is the groove spacing of the grating.

Assuming that a lens of focal length f is used in the receiving collimator, we can calculate B from

$$\cos(B) = \frac{f(\Delta\lambda/D)}{d}, \tag{6}$$

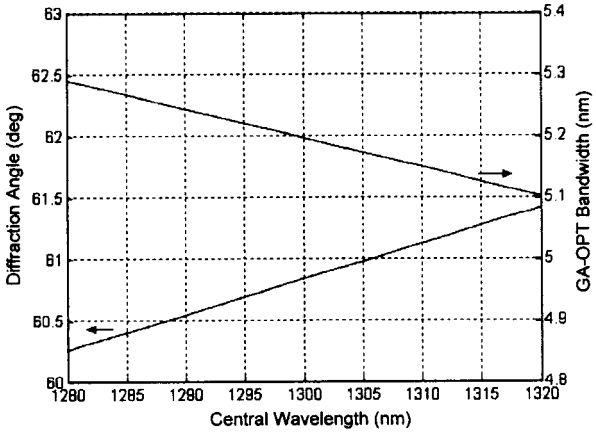

Fig. 3. Wavelength dependence of the diffraction angle and GA-OPT bandwidth (Δλ).

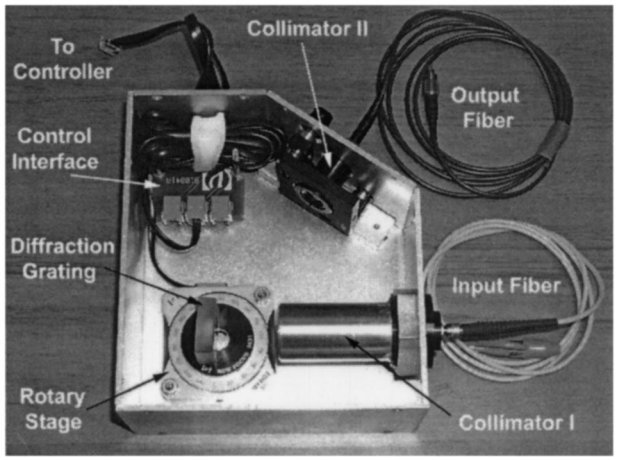

Fig. 4. Top view of GA-OPT.

where Δλ is the spectrum resolution and D is the diameter of the core of the receiving MMF or the active area of the detector.

With λ = 1300 nm, d = 1/750 mm, f = 25.0 mm, D = 0.2 mm for a 200–2300-μm MMF, and B–A = 55°, Fig. 3 gives the calculated angular tuning range for wavelength tuning from 1280 to 1320 nm and the resultant change in receiving bandwidth. An angular change of 1.2° is enough for scanning a wavelength range of 40 nm, and a bandwidth error of ~3.5% may result. This bandwidth error may induce an error in the optical intensity distribution from the original light source distribution that one can easily compensated for by scanning the whole spectrum range and storing the new intensity distribution during the reset. Obviously, finer tuning or smaller Δλ can be achieved, with a penalty of higher insertion loss, by use of smaller-diameter fiber D or a longer focal length f if the groove spacing, incident angle A, and diffraction angle B have been determined.

4. Experiments

To verify the feasibility of operation-point tuning we designed and fabricated GA-OPT, as shown in Fig. 4. A holographic diffraction grating of 750 grooves/mm was glued onto a motorized rotary stage. The motor has a step resolution of 0.2 mrad and a rotation speed of 2 rpm, which means that a central wavelength resolution of 0.38 nm and a tuning speed of 400 nm/s can be achieved. Collimator I is the input collimator, and collimator II is the output collimator, which has a focal length of 25 mm. The input SMF is connected to an interferometric optical sensor, and the output 200–230-μm MMF is connected to an optical receiver. The control interface board interconnects the motor and the motor controller.

In Fig. 5 are shown the spectra received by the detector at various grating positions or central wavelengths (1276.4, 1288.0, 1298.0, 1307.9, and 1317.9 nm) and the original spectrum of the superluminescent light-emitting diode (SLED), where the sensor was replaced with a cleaved SMF. A 1296-nm SLED with a spectral width of 35 nm was used as the broadband source. Scanning the grating at an angle of 1.2° achieved a central wavelength change of 40 nm. This agrees well with the theoretical calculation given in Fig. 3. The resultant spectrum bandwidth (FWHM) is 4.30–4.65 nm, an average of 0.7 nm less than the theoretical results. This difference is believed to be caused by misalignment between the 25-mm lens in collimator II and the 200–230-μm MMF as well as by the relatively small aperture of collimator II. The total insertion loss is ~11 dB. As mentioned in Section 3, a trade-off must be made between large bandwidth for high optical power and small bandwidth for high fringe visibility and high resolution of operation-point tuning.

The wavelength scan outputs of a FFPI sensor and the theoretical results in atmospheric pressure are shown in Fig. 6(a). The peak amplitudes are unequal because of the Gaussian spectrum distribution of the 1296-nm SLED source. The peak position differences between the experimental results and the

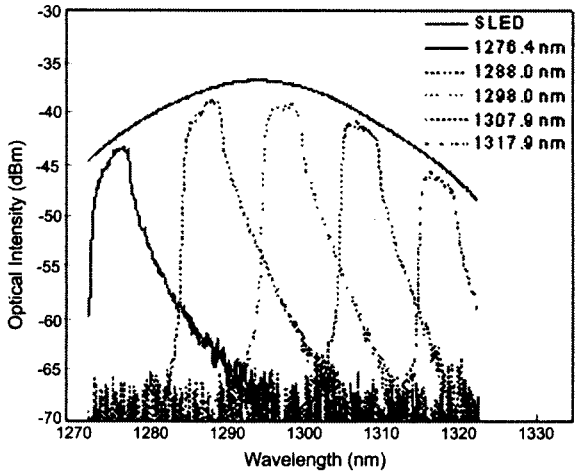

Fig. 5. Spectra received by the detector at several grating positions and the original spectrum of the SLED.

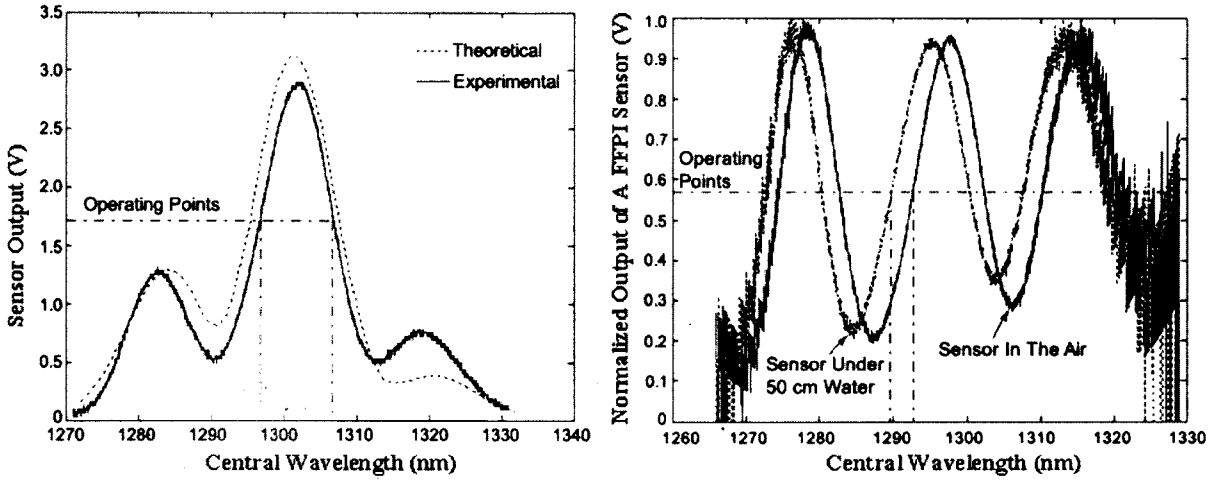

Fig. 6. Output of a FFPI sensor: (a) theoretical result and sensor output, (b) normalized sensor outputs at different static pressures.

theoretical calculation are caused by cavity-length measurement error, whereas the amplitude differences are believed to be caused by the offset of the spectrum distribution from the ideal Gaussian distribution used for the calculation and by misalignment of GA-OPT or of the sensor's F-P cavity. Figure 6(b) gives the scan outputs of a FFPI sensor in the atmospheric environment and under 50 cm of water normalized to the source spectrum. A Q-point drift of $\sim$3 nm resulted from the 50-cm static water pressure. Obviously there is more than one Q point on the fringes, but only those two Q points on the highest fringe have the best signal-to-noise ratio and thereby are suitable as optimal operation points.

A diaphragm-based FFPI acoustic-wave sensor[11] was chosen to test the performance of the developed GA-OPT in practical applications. This sensor was designed for partial-discharge detection in power transformers. Because this sensor was fabricated by use of thermal fusion bonding, which might cause large cavity-length error and may suffer from high static pressure in a transformer tank full of mineral oil, operation point control has been a major challenge, and very low sensitivity may result. A scan output of this sensor in an acoustic-wave test setup is given in Fig. 7(a). The acoustic-wave outputs at marked points A–E in Fig. 7(a) are shown in Fig. 7(b), along with that from a sensor system without GA-OPT. Obviously, the original system has a low signal-to-noise ratio (SNR) because of the short coherence length of the SLED source compared with the sensor's cavity length, the unknown operation point, or both. When GA-OPT is used, the sensor performs differently at different operation points. At points A and C the Q points of the interference fringes, the sensor has the best SNR, which is attributed to the highest sensitivity of the Q point and the increased fringe contrast. An improvement of $\sim$15 dB in SNR compared with that of the original sensor can easily be achieved, even if the original sensor was operating at its Q point. The sensor's SNR has only moderate improvement at points D and E, though they are Q points too, because of the lower fringe slope at D or the low absolute optical intensity at E, both caused by the nonflat SLED spectrum. The

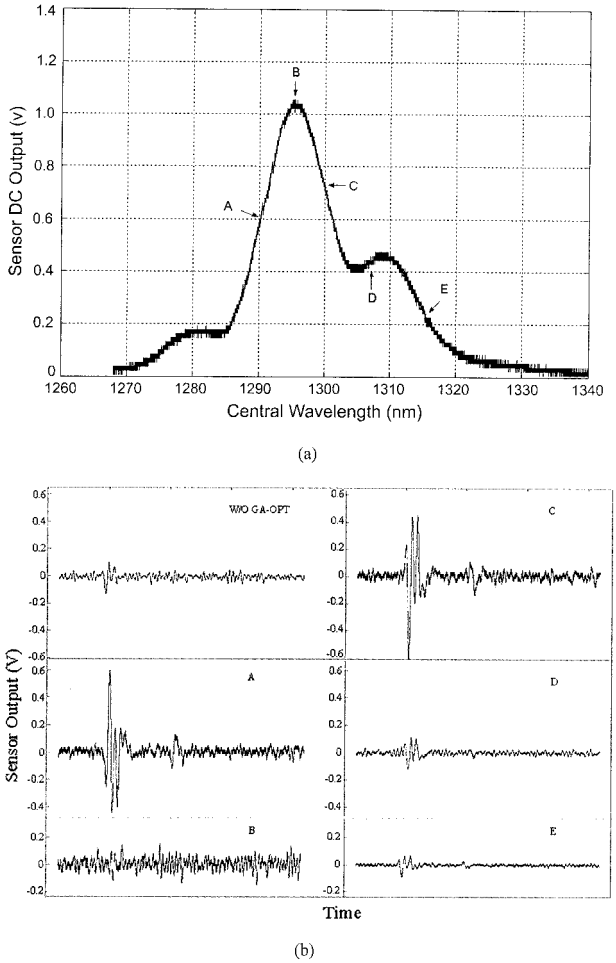

Fig. 7. Acoustic wave detection with a diaphragm-based FFPI sensor and GA-OPT: (a) scanning for the operation point, (b) acoustic-wave outputs without (WO) GA-OPT and with GA-OPT but at different operation points.

sensor has the lowest SNR at B because of the zero sensitivity at the fringe peaks (or valleys). Therefore points A and C are the ideal operation points of this FFPI sensor. We also observed that the acoustic-wave outputs at these two points have different polarities and different dynamic ranges that may be sensitive for some measurements. When the operation point is determined, the last task is to maintain the sensor operation at the setting point. This can easily be achieved by the feedback-control system shown in the system diagram of Fig. 2. A signal-processing system that uses a computer and a data-acquisition card makes data recording and calibration easy and fast.

5. Discussion

In conclusion, an effective demodulation technique has been developed for dynamic compensation of manufacturing errors and environmental-perturbation-induced drifts in interferometric sensors. The total effect of all low-frequency drifts, including dc signals, in the sensor system can be measured by the position of the diffraction grating. The dc signals may be recoverable if other effects, such as temperature, are known or can be measured. If such is the case, the dc dynamic range of the sensor system can be greatly increased and is limited only by the source bandwidth. Obviously, the GA-OPT does not impose any limit on the ac signal, and the frequency response of the sensor system depends only on the sensor probe itself and the electronic bandwidth.

In addition to operation-point control, GA-OPT brings another benefit to the demodulation system, namely, improved sensitivity. The improvement comes from the reduction of the bandwidth of the interrogation lights and thereby from the increase of the interference fringe contrast.[11] Although the fringe contrast is still smaller than that of a sensor system with a laser source, this demodulation approach retains all the advantages of a white-light system over a laser system.

The potential for absolute OPD measurements is another important feature of GA-OPT. By scanning the wavelength, one may calculate the absolute OPD between the sensing channel and the reference channel from the scanning output, as was done by Egorov *et al*. with a spectrometer and a CCD array.[16] Compared with the method described in Ref. 16, the advantage of the GA-OPT is greatly reduced cost, especially for sensors operating in the near-infrared region.

This research was supported by the U.S. Department of Energy under contract DE-FC-01GO11050. The authors acknowledge useful discussions with Yibing Zhang of the Center for Photonics Technology, Virginia Polytechnic Institute and State University.

References

1. T. Yoshino, K. Kurosawa, K. Itoh, and T. Ose, "Fiber-optic Fabry–Perot interferometer and its sensor application," IEEE Trans. Microwave Theory Tech. **MTT-30,** 1612–1620 (1982).
2. C. E. Lee and H. F. Taylor, "Fiber-optic Fabry–Perot temperature sensor using a low-coherence light source," J. Lightwave Technol. **9,** 129–134 (1991).
3. R. A. Wolthuis, G. L. Mitchell, E. Saaski, J. C. Hartl, and M. A. Afromowitz, "Development of medical pressure and temperature sensors employing optical spectrum modulation," IEEE Trans. Biomed. Eng. **38,** 974–981 (1991).
4. A. Wang, H. Xiao, J. Wang, Z. Wang, W. Zhao, and R. G. May, "Self-calibrated interferometric-intensity-based optical fiber sensors," J. Lightwave Technol. **19,** 1495–1501 (2001).
5. N. Furstenau, M. Schmidt, H. Horack, W. Goetze, and W. Schmidt, "Extrinsic Fabry–Perot interferometer vibration and acoustic sensor systems for airport ground traffic monitoring," IEE Proc. Optoelectron. **144,** 134–144 (1997).
6. W. Pulliam, P. Russler, R. Mlcak, K. Murphy, and C. Kozikowski, "Micromachined, SiC fiber optic pressure sensors for high temperature aerospace applications," in *Industrial Sensing Systems*, A. Wang and E. Udd, eds., Proc. SPIE **4202,** 21–30 (2000).
7. Y. Kim and D. P. Neikirk, "Micromachined Fabry–Perot cavity pressure transducer," IEEE Photon. Technol. Lett. **7,** 1471–1473 (1995).
8. J. J. Alcoz, C. E. Lee, and H. F. Taylor, "Embedded fiber-optic Fabry–Perot ultrasound sensor," IEEE Trans. Ultrason. Ferroelectr. Freq. Control **37,** 302–306 (1990).
9. J. F. Dorighi, S. Krishnaswamy, and J. Achenbach, "Stabilization of an embedded fiber optic Fabry–Perot sensor for ultrasound detection," IEEE Trans. Ultrason. Ferroelectr. Freq. Control **42,** 820–824 (1995).
10. K. A. Murphy, M. F. Gunther, A. Wang, and R. O. Claus, "Detection of acoustic emission location using optical fiber sensors," in *Smart Structures and Materials 1994: Smart Sensing, Processing, and Instrumentation*, J. S. Sirkis, ed., Proc. SPIE **2191,** 282–290 (1994).
11. B. Yu, D. W. Kim, J. Deng, H. Xiao, and A. Wang, "Fiber Fabry–Perot sensors for partial discharge detection in power transformers," Appl. Opt. **42,** 3241–3250 (2003).
12. K. Murphy, M. F. Gunther, A. M. Vengsakar, and R. O. Claus, "Quadrature phase-shifted, extrinsic Fabry–Perot optical fiber sensors," Opt. Lett. **16,** 273–275 (1991).
13. C. Belleville and G. Duplain, "White-light interferometric multimode fiber-optic strain sensor," Opt. Lett. **18,** 78–80 (1993).
14. A. S. Gerges, F. Farahi, T. P. Newson, J. D. C. Jones, and D. A. Jackson, "Fibre-optic interferometric sensor utilising low coherence length sources: resolution enhencement," Electron. Lett. **24,** 472–474 (1988).
15. M. Schmidt and N. Fürstenau, "Fiber-optic extrinsic Fabry–Perot interferometer sensors with three-wavelength digital phase demodulation," Opt. Lett. **24,** 599–601 (1999).
16. S. A. Egorov, A. N. Mamaev, I. G. Likhachiev, Y. A. Ershov, A. S. Voloshin, and E. Nir, "Advanced signal processing method for interferometric fiber-optic sensors with straightforward spectral detection," in *Sensors and Controls for Advanced Manufacturing*, B. O. Nnaji and A. Wang, eds., Proc. SPIE **3201,** 44–48 (1998).
17. B. Qi, G. Pickrell, J. C. Xu, P. Zhang, Y. H. Duan, W. Peng, Z. Y. Huang, W. Huo, H. Xiao, R. G. May, and A. Wang, "Novel date processing techniques for dispersive white light interferometer," Optical Engineering (to be published).